Electrocatalysis

DOI: 10.1002/anie.201410792

Palladium–Cobalt Nanotube Arrays Supported on Carbon Fiber Cloth as High-Performance Flexible Electrocatalysts for Ethanol Oxidation**

*An-Liang Wang, Xu-Jun He, Xue-Feng Lu, Han Xu, Ye-Xiang Tong, and Gao-Ren Li**

Abstract: *PdCo nanotube arrays (NTAs) supported on carbon fiber cloth (CFC) (PdCo NTAs/CFC) are presented as high-performance flexible electrocatalysts for ethanol oxidation. The fabricated flexible PdCo NTAs/CFC exhibits significantly improved electrocatalytic activity and durability compared with Pd NTAs/CFC and commercial Pd/C catalysts. Most importantly, the PdCo NTAs/CFC shows excellent flexibility and the high electrocatalytic performance remains almost constant under the different distorted states, such as normal, bending, and twisting states. This work shows the first example of Pd-based alloy NTAs supported on CFC as high-performance flexible electrocatalysts for ethanol oxidation.*

Recently, portable and flexible electronic devices, such as the roll-up displays, wearable devices, and small mobile devices, have attracted great attention because of their lightweight, bendable, and wearable nature.[1] The rapid development of flexible and portable electronics has prompted demands for flexible and lightweight energy sources. Fuel cells, which have advantages of efficient energy conversion, being clean, security, high energy density, and low maintenance, are a promising power source.[2–5] Accordingly flexible fuel cells will attract great interest and will be an excellent candidate for the portable and flexible electronics.[6] As a flexible electrochemical device, a prerequisite is that every part should be made with flexible material. Therefore, it is highly interesting and urgent to investigate the flexible electrocatalysts for the development of flexible fuel cells.

Conventional electrocatalysts of fuel cells are mainly divided into two categories: one kind is binder-free and the catalyst directly grow on current collector, such as Ti sheet,[7] porous gold,[8] and ITO sheet;[9] another kind needs binder to glue catalyst on the surface of current collector.[10–12] For most studies, the glass carbon (GC) electrode was used as a current collector.[13–15] The catalyst was firstly dropped on the surface of GC electrode, then the binder-Nafion or PTFE (polytetrafluoroethene) was spread over the surface to immobilize the catalyst. In the above studies, although the electrocatalysts showed high electrocatalytic performance, the non-flexibility of current collectors (such as Ti sheet, FTO, ITO, and GC) obviously hinder the study of flexible electrocatalysts.[16–18] Recently, some inorganic materials grown on flexible supports, such as carbon cloth,[19] graphene paper,[20] graphene foams,[21] paper,[22] and nickel foam,[23] have been widely reported as the flexible electrodes for supercapacitors, Li-ion batteries, and organic photovoltaics. The reported electrodes exhibited excellent mechanical flexibility and the different bending states of electrodes almost did not affect their electrochemical performance. However, so far there almost has been no report on the flexible electrocatalysts for fuel cells.

Herein, we first studied PdCo nanotube arrays (NTAs) supported on carbon fiber cloth (CFC) (PdCo NTAs/CFC) as flexible electrocatalysts for ethanol oxidation for direct ethanol fuel cells (DEFCs). The CFC has excellent flexibility, high conductivity, and a large surface area. Here the PdCo NTAs directly grow on CFC by template-assisted electrodeposition method, and the binder is not needed. The PdCo NTAs/CFC are a prime example of flexible electrocatalysts with well-defined multiple nanostructures, and they show following advantages: 1) the NTAs and CFC will provide large surface area, fast electrolyte penetration/diffusion because of the hollow and porous structures; 2) the NTAs/CFC will be much less vulnerable to dissolution, Ostwald ripening, and aggregation, which is beneficial to the improvement of stability of the catalysts; 3) as the CFC is highly flexible, the PdCo NTAs/CFC electrocatalyst have excellent flexibility and show great potential for flexible fuel cell devices; 4) the optimization of the Pd and Co atom ratio can be easily realized in the PdCo NTAs by electrodeposition method and accordingly the electrocatalytic performance can be significantly improved. The electrochemical measurements demonstrate that the synthesized PdCo NTAs/CFC exhibits high electrocatalytic activity and durability for ethanol oxidation. What is more, we demonstrate that the PdCo NTAs/CFC has excellent flexibility and its electrocatalytic activity, cycling durability, and CO stripping ability are almost completely unaffected by the different bending states, indicating promising prospects for flexible fuel cell devices.

Scheme 1 shows the fabrication procedures of PdCo NTAs/CFC; the details are described in the Experimental

[*] A.-L. Wang, X.-J. He, X.-F. Lu, H. Xu, Y.-X. Tong, Prof. G.-R. Li
MOE Laboratory of Bioinorganic and Synthetic Chemistry
KLGHEI of Environment and Energy Chemistry
School of Chemistry and Chemical Engineering
Sun Yat-sen University, Guangzhou 510275 (China)
E-mail: ligaoren@mail.sysu.edu.cn

[**] This work was supported by the NSFC (51173212 and 21476271), NSFGP (S2013020012833), Fundamental Research Fund for the Central Universities (13lgpy51), SRF for ROCS, SEM ((2012)1707), New-Century Training Programme Foundation for the Talents by the State Education Commission (NCET-12-0560), and Open-End Fund of Key Laboratory of Functional Inorganic Material Chemistry (Heilongjiang University), Ministry of Education.

Supporting information for this article is available on the WWW under http://dx.doi.org/10.1002/anie.201410792.

 © 2015 Wiley-VCH Verlag GmbH & Co. KGaA, Weinheim

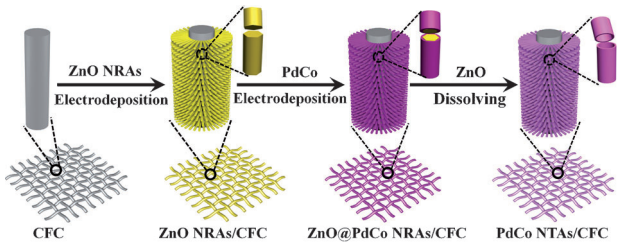

Scheme 1. Representation of the fabrication of PdCo NTAs/CFC by ZnO template-assisted electrodeposition.

Section in the Supporting Information. Here the CFC is used as a support (or current collector). A SEM image of the CFC is shown in the Supporting Information, Figure S1, and it is clear that the CFC consists of carbon fibers with diameters of about 7 μm. ZnO nanorod arrays (NRAs) are first coated on the surface of CFC to form ZnO NRAs/CFC, and they perpendicularly stand around the carbon fiber (Supporting Information, Figure S2). The diameters and lengths of ZnO nanorods are about 300 nm and 3.0 μm, respectively. Then PdCo alloys were further coated on the surfaces of ZnO NRAs to form ZnO@PdCo NRAs/CFC. It can be clearly seen that the PdCo alloy wraps favorably share the surfaces of ZnO NRAs and almost no deposit is packed into the interspaces of ZnO nanorods (Supporting Information, Figure S3). After dissolving ZnO, the PdCo NTAs/CFC was fabricated, and it shows excellent flexibility (Supporting Information, Figure S4). SEM images of the PdCo NTAs/CFC with different magnifications are shown in Figure 1 a,b, which shows PdCo nanotubes uniformly stand on the surface of CFC and they are separate with each other. The magnified SEM image of a typical PdCo nanotube is shown in Figure 1 c, which shows that the outer surface of PdCo nanotube consists of many nanosheets, and thus will obviously further enhance the surface area of catalysts. The EDX mapping is measured on the PdCo nanotube to investigate the distributions of Pd and Co. The corresponding EDX maps of elements Co and Pd are shown in Figure 1 d and e, respectively, which show that the elements Co and Pd are both well-dispersed in the PdCo nanotubes. The Pd/Co atomic ratio in PdCo NTAs is determined to be about 0.23.

To confirm the hollow structure, a TEM image of a PdCo nanotube was obtained (Figure 1 f), which clearly shows the hollow structure and the nanotube surface is made of many nanosheets. The thickness of nanotube wall is about 50 nm. Obviously the hollow structure and nanosheets on the outer surface of PdCo NTAs will offer a large void space, which will be beneficial for mass transport of reactant and resultant molecules and will obviously enhance the utilization rate of electrocatalysts. A HRTEM image and SAED pattern of PdCo NTAs were also measured and typical results are shown in Figure 1 g, which shows amorphous structures of PdCo nanoparticles. An XRD pattern of PdCo NTAs/CFC is shown in the Supporting Information, Figure S5, and no peak is seen apart from the peaks of CFC. This can be attributed to amorphous PdCo alloys in the sample.

To investigate the effect of Co on the electron structure of Pd, an XPS spectra of PdCo NTAs/CFC and Pd NTAs/CFC in the Pd 3d regions were measured (Figure 2 a). Each Pd 3d

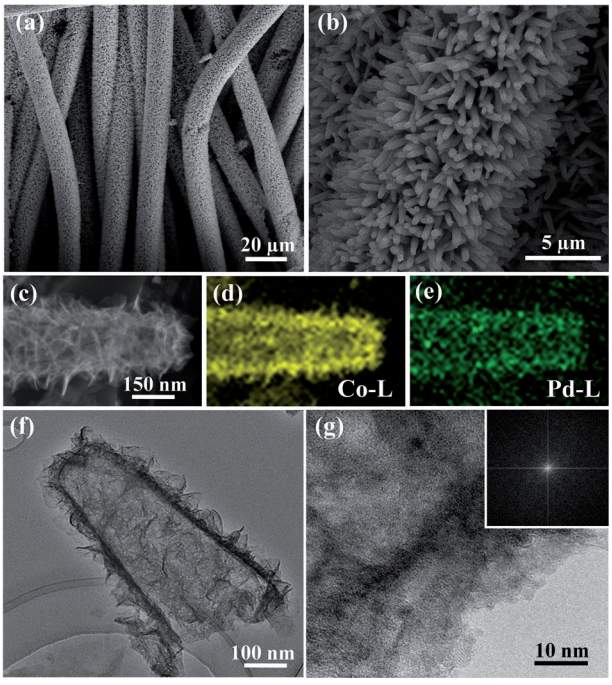

Figure 1. a,b) SEM images of PdCo NTAs/CFC at different magnifications; c) SEM image of a typical PdCo nanotube; d) Co elemental mapping in the PdCo nanotube; e) Pd elemental mapping in the PdCo nanotube; f) TEM image of a typical PdCo nanotube; g) HRTEM image and SAED pattern (inset) of PdCo nanotube.

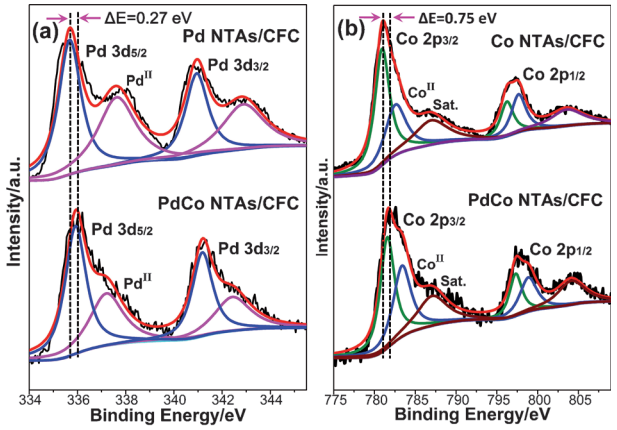

Figure 2. XPS spectra of a) Pd 3d and b) Co 2p performed on the PdCo NTAs/CFC, Pd NTAs/CFC, and Co NTAs/CFC.

peak can be deconvoluted into two pairs of doublets. A comparison of the relative areas of integrated intensity of Pd^0 and Pd^{II} shows that plentiful Pd exists as Pd^{II} in the Pd NTAs/CFC catalyst, while less Pd^{II} is observed in the PdCo NTAs/CFC catalyst, indicating that the introduction of Co can significantly increase relative content of Pd^0 in the PdCo NTAs/CFC catalyst. Further, Figure 2 a shows that the Pd $3d_{5/2}$ and $3d_{3/2}$ peaks of PdCo NTAs both shift to higher binding energies (335.94 and 341.21 eV) relative to the Pd $3d_{5/2}$ and

© 2015 Wiley-VCH Verlag GmbH & Co. KGaA, Weinheim

$3d_{3/2}$ peaks of Pd NTAs/CFC (335.67 and 340.94 eV). The positive shifts (ca. 0.27 eV) of Pd peaks in binding energies confirm the strong electron interactions involving Pd and Co in the PdCo NTAs. Further, Figure 2b shows that the Co $2p_{3/2}$ and $2p_{1/2}$ peaks of PdCo NTAs both shift to higher binding energies relative to Co $2p_{3/2}$ and $2p_{1/2}$ peaks of Co NTAs/CFC. The positive shifts (ca. 0.75 eV) of Co peaks in the binding energies also confirm the strong electron interactions involving Pd and Co in the PdCo NTAs. The electron interactions between Pd and Co will obviously alter electronic states of Pd atoms and accordingly will possibly improve the electrocatalytic activity and durability of PdCo NTAs.

The PdCo NTAs/CFC electrocatalyst was firstly evaluated by the electrochemically active surface area (ECSA) that is an important parameter for the assessment of electrochemically active sites of electrocatalysts. The ESCA of PdCo NTAs/CFC can be calculated from the area of the reduction peak of PdO. Figure 3a shows CVs of PdCo NTAs/CFC, Pd NTAs/CFC, and Pd/C catalysts in the deaerated KOH solution (1.0 M) at 50 $mV s^{-1}$. The ECSA (m^2/g_{Pd}) of the catalysts is estimated according to the equation ECSA $= Q/(0.405 \times W_{Pd})$, where W_{Pd} represents Pd loading (mg/cm^2) on the electrode, Q is the coulombic charge by integrating peak area of the reduction of PdO (mC), and 0.405 represents the charge required for the reduction of PdO monolayer (mC/cm^2_{Pd}).[24] Herein, the ESCA of PdCo NTAs/CFC is calculated to be 50.13 $m^2 g^{-1}$, which is remarkably larger than those of Pd NTAs/CFC (28.11 $m^2 g^{-1}$) and commercial Pd/C catalysts (23.82 $m^2 g^{-1}$). The enhancement in ESCA of PdCo NTAs/CFC can be attributed to hollow nanotube structure, hierarchical structure in the walls of PdCo nanotubes, high content of metallic Pd, and the effect of Co on the electronic state of Pd.

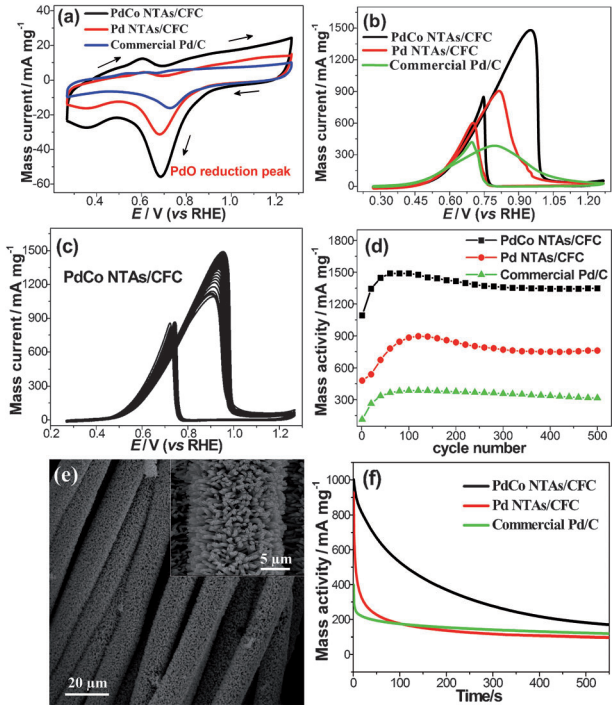

Figure 3. a) CVs of PdCo NTAs/CFC, Pd NTAs/CFC, and commercial Pd/C in 1.0 M KOH solution at 50 $mV s^{-1}$; b) CVs of PdCo NTAs/CFC, Pd NTAs/CFC, and commercial Pd/C in 1.0 M KOH + 1.0 M C_2H_5OH at 50 $mV s^{-1}$; c) CVs of PdCo NTAs/CFC from 1 st to 500th cycle in solution of 1.0 M KOH + 1.0 M C_2H_5OH at 50 $mV s^{-1}$; d) The cycling stability of peak current densities of PdCo NTAs/CFC, Pd NTAs/CFC, and commercial Pd/C with increasing cycles; e) SEM image of PdCo NTAs/CFC after 500 cycles; f) Chronoamperometry curves measured in 1.0 M KOH + 1.0 M C_2H_5OH at 50 $mV s^{-1}$ (the corresponding potential was held at 0.77 V during the measurements).

Electrocatalytic activities of PdCo NTAs/CFC, Pd NTAs/CFC and commercial Pd/C catalysts for ethanol oxidation were investigated in the solution of 1.0 M KOH + 1.0 M C_2H_5OH at 50 $mV s^{-1}$, and the representative CVs are shown in Figure 3b. The mass peak current density (normalized to the mass of Pd) of PdCo NTAs/CFC is almost 1.7 times higher than that of Pd/CFC NTAs and 4 times higher than that of commercial Pd/C, indicating PdCo NTAs/CFC have a much higher mass catalytic activity than Pd NTAs/CFC and commercial Pd/C. Among the potentials of 0.81–0.99 V, the PdCo NTAs/CFC always shows much higher mass activity than Pd NTAs/CFC and commercial Pd/C at a certain potential. Furthermore, when the current densities all are normalized to the ECSAs of catalysts, the PdCo NTAs/CFC shows circa 1.15 and circa 2.28 times higher current density than Pd NTAs/CFC and commercial Pd/C catalysts, respectively, as shown in the Supporting Information, Figure S7, indicating the PdCo NTAs/CFC also have a higher ECSA catalytic activity than Pd NTAs/CFC and commercial Pd/C catalysts. Herein, we also studied the effect of the compositions of PdCo NTAs on catalytic activity of catalysts. CVs of PdCo NTAs/CFC catalysts with different contents of Pd in the solution of 1.0 M C_2H_5OH + 1.0 M KOH at 50 $mV s^{-1}$ are shown in the Supporting Information, Figure S9, and the summary of mass peak current densities is shown in the Supporting Information, Table S2. It is clear to see that the mass catalytic activity reaches to the maximum when the ratio of Pd/Co in PdCo NTAs/CFC is 0.23.

Figure 3c shows various CVs of PdCo NTAs/CFC with increasing cycle number in the solution of 1.0 M KOH + 1.0 M C_2H_5OH at 50 $mV s^{-1}$, and the change of peak current density versus cycle number is shown in the Figure 3d. The catalytic activity of PdCo NTAs/CFC has an increase in the initial cycles and the maximum peak current density appears at the 60th cycle. After the 60th cycle, the peak current density exhibits a slow attenuation with further increasing cycle number. After 500 cycles, the conservation rate of peak current density is about 90.6% of the maximum value, indicating that the PdCo NTAs/CFC have superior cycling stability for ethanol electrooxidation. Compared with PdCo NTAs/CFC, the Pd NTAs/CFC and commercial Pd/C catalysts exhibit lower conservation rates of the maximum peak current densities (84.9% and 81.6%, respectively) after 500 cycles as shown in Figure 3d. Therefore, the PdCo NTAs/CFC exhibit enhanced cycling stability compared with the Pd NTAs/CFC and commercial Pd/C catalysts. Furthermore, Figure 3d also shows PdCo NTAs/CFC catalyst owns much higher catalytic activity than Pd NTAs/CFC and commercial Pd/C catalysts during 500 cycles. After 500 cycles, the

 © 2015 Wiley-VCH Verlag GmbH & Co. KGaA, Weinheim

morphology of PdCo NTAs/CFC is still maintained very well as shown in the Figure 3e, indicating the excellent structure stability of PdCo NTAs/CFC.

To further evaluate the electrocatalytic activity and stability of the PdCo NTAs/CFC catalyst, chronoamperometric experiments of PdCo NTAs/CFC, Pd NTAs/CFC, and commercial Pd/C catalysts were carried out in 1.0 M ethanol + 1.0 M KOH solution (Figure 3f). The potential was held at 0.77 V during the measurements. It is found that the mass current density of PdCo NTAs/CFC is always much higher than those of Pd NTAs/CFC and commercial Pd/C catalysts, further demonstrating that the PdCo NTAs/CFC owns a significantly enhanced electrocatalytic activity. This result is in agreement with the CVs shown in Figure 3b. Furthermore, the PdCo NTAs/CFC shows much slower current decay over time than Pd NTAs/CFC and Pd/C catalysts, indicating that the PdCo NTAs/CFC catalyst has a much better durability for ethanol oxidation.

To develop the flexible electrocatalysts, the catalytic performance should be kept unchanged under the different bending states. Herein, the effect of the flexibility of PdCo NTAs/CFC on ESCA and catalytic activity is studied. To investigate the ESCA of PdCo NTAs/CFC at the different distorted states, CVs at the normal, bending, and twisting states were measured in the deaerated KOH solution (1.0 M) at 50 mV s^{-1} (Figure 4a). It is clear to see that the CVs of

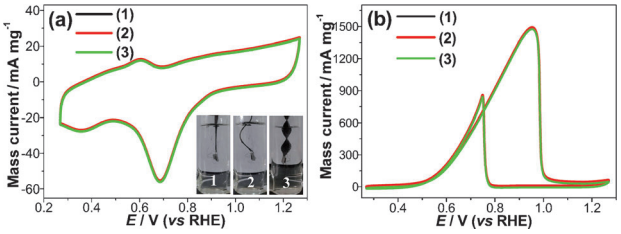

Figure 4. a) CVs of PdCo NTAs/CFC in 1.0 M KOH solution at 50 mV s^{-1} at different distorted states: 1) normal, 2) bending, 3) twisting; b) CVs of PdCo NTAs/CFC in solution of 1.0 M KOH + 1.0 M C_2H_5OH at 50 mV s^{-1} at the different distorted states given in (a).

PdCo NTAs/CFC almost keep the same under the different states of normal, bending, and twisting. Furthermore, CVs of PdCo NTAs/CFC at different bending states were measured in the solution of 1.0 M KOH + 1.0 M C_2H_5OH at 50 mV s^{-1} (Figure 4b), which also shows the CVs almost keep the same under the different bending states. Therefore, the above results indicate that the PdCo NTAs/CFC is an excellent flexible electrocatalyst, and its ESCA and electrocatalytic activity almost are not affected by the different bending states.

To evaluate CO antipoisoning ability of PdCo NTAs/CFC, CO oxidation experiments were carried out at room temperature in the solution of 1.0 M KOH that was purged with nitrogen for 30 min and then was bubbled with CO gas (99.99%) for 15 min. The potential was kept at 0.27 V to achieve the maximum coverage of CO at the Pd active centers. The residual CO in the solution was excluded by N_2 (99.99%) for 20 min. Figure 5a shows two consecutive CVs of

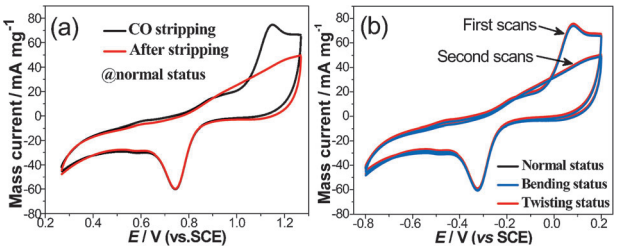

Figure 5. a) CO stripping voltammograms on the PdCo NTAs/CFC performed in solution of 1.0 M KOH at 50 mV s^{-1}; b) CO stripping voltammograms on the PdCo NTAs/CFC performed in solution of 1.0 M KOH at 50 mV s^{-1} in the normal, bending, and twisting states.

PdCo NTAs/CFC recorded within the potentials between 0.27 and 1.27 V at 50 mV s^{-1} in the saturated CO solution of 1.0 M KOH. In the first forward scan, it is clear to see that a large CO oxidation peak appears. On the second forward scan, the CO oxidation peak disappears owing to the complete elimination of CO on the surface of catalyst, indicating high CO antipoisoning ability of PdCo NTAs/CFC. To investigate the effect of flexibility of PdCo NTAs/CFC on CO antipoisoning ability under the different distorted states, the CO oxidation measurements were carried out at the normal, bending, and twisting states of PdCo NTAs/CFC in the saturated CO solution of 1.0 M KOH as shown in the Figure 5b, which shows the CVs of the first scans almost are the same and those of the second scans are also the same too. Therefore, the CO antipoisoning ability of PdCo NTAs/CFC electrocatalyst is almost not affected by the different distorted states.

In conclusion, we have demonstrated an electrodeposition strategy for the fabrication of novel flexible PdCo NTAs/CFC electrocatalysts. The PdCo NTAs/CFC catalysts exhibit significantly enhanced electrocatalytic activity and cycling stability towards ethanol oxidation, indicating promising potential of PdCo NTAs/CFC for DEFCs. Most importantly, because of invariant performance under the various distorted states, such as normal, bending, and twisting states, the PdCo NTAs/CFC provides a fundamental opportunity for the development of flexible electrocatalysts. Considering the excellent performance and flexibility of PdCo NTAs/CFC, the present encouraging findings might open up a new avenue for the development of high-performance flexible Pd-based alloy NTAs/CFC catalysts for fuel cells.

Received: November 5, 2014
Revised: December 13, 2014
Published online: February 4, 2015

Keywords: carbon fiber cloth · electrocatalysts · ethanol oxidation · nanotube arrays · PdCo alloy

[1] L. Li, L. Z. Wu, S. Yuan, X. Zhang, *Energy Environ. Sci.* **2014**, *7*, 2101.
[2] a) Y. Hsieh, Y. Zhang, D. Su, V. Volkov, R. Si, L. Wu, Y. Zhu, W. An, P. Liu, P. He, S. Ye, R. Adzic, J. X. Wang, *Nat. Commun.* **2013**, *4*, 2466; b) D. Wang, H. Xin, R. Hovden, H. Wang, Y. Yu, D. Muller, F. DiSalvo, H. D. Abruña, *Nat. Mater.* **2013**, *12*, 81;

 © 2015 Wiley-VCH Verlag GmbH & Co. KGaA, Weinheim

c) W. Zhang, Z. Wu, H. Jiang, S.-H. Yu, *J. Am. Chem. Soc.* **2014**, *136*, 14385.
[3] a) M. Gao, W. Sheng, Z. Zhuang, Q. Fang, S. Gu, J. Jiang, Y. Yan, *J. Am. Chem. Soc.* **2014**, *136*, 7077; b) S. W. Kang, Y. W. Lee, Y. Park, B.-S. Choi, J. W. Hong, K.-H. Park, S. W. Han, *ACS Nano* **2013**, *7*, 7945; c) Y. Jia, Y. Jiang, J. Zhang, L. Zhang, Q. Chen, Z. Xie, L. Zheng, *J. Am. Chem. Soc.* **2014**, *136*, 3748.
[4] a) B. T. Sneed, C.-H. Kuo, C. N. Brodsky, C.-K. Tsung, *J. Am. Chem. Soc.* **2012**, *134*, 18417; b) C. Zhu, S. Guo, S. Dong, *Adv. Mater.* **2012**, *24*, 2326; c) B. Y. Xia, H. B. Wu, Y. Yan, X. W. Lou, X. Wang, *J. Am. Chem. Soc.* **2013**, *135*, 9480.
[5] a) J. Suntivich, Z. Xu, C. E. Carlton, J. Kim, B. Han, S. W. Lee, N. Bonnet, N. Marzari, L. F. Allard, H. A. Gasteiger, K. Hamad-Schifferli, Y. Shao-Horn, *J. Am. Chem. Soc.* **2013**, *135*, 7985; b) M. Li, D. Cullen, K. Sasaki, N. S. Marinkovic, K. More, R. R. Adzic, *J. Am. Chem. Soc.* **2013**, *135*, 132.
[6] M. Winter, R. J. Brodd, *Chem. Rev.* **2004**, *104*, 4245.
[7] A.-L. Wang, H. Xu, J.-X. Feng, L.-X. Ding, Y.-X. Tong, G.-R. Li, *J. Am. Chem. Soc.* **2013**, *135*, 10703.
[8] R. Wang, C. Wang, W.-B. Cai, Y. Ding, *Adv. Mater.* **2010**, *22*, 1845.
[9] B.-S. Choi, Y. W. Lee, S. W. Kang, J. W. Hong, J. Kim, I. Park, S. W. Han, *ACS Nano* **2012**, *6*, 5659.
[10] a) C. Xu, H. Wang, P. Shen, S. Jiang, *Adv. Mater.* **2007**, *19*, 4256; b) C. Hu, H. Cheng, Y. Zhao, Y. Hu, Y. Liu, L. Dai, L. Qu, *Adv. Mater.* **2012**, *24*, 5493; c) A. Leelavathi, G. Madras, N. Ravishankar, *J. Am. Chem. Soc.* **2014**, *136*, 14445.
[11] a) B. T. Sneed, A. P. Young, D. Jalalpoor, M. C. Golden, S. Mao, Y. Jiang, Y. Wang, C.-K. Tsung, *ACS Nano* **2014**, *8*, 7239; b) W. Du, G. Yang, E. Wong, N. A. Deskins, A. I. Frenkel, D. Su, X. Teng, *J. Am. Chem. Soc.* **2014**, *136*, 10862; c) C. Zhang, S. Y. Hwang, A. Trout, Z. Peng, *J. Am. Chem. Soc.* **2014**, *136*, 7805.
[12] a) Y. Zhang, M. Janyasupab, C.-W. Liu, X. Li, J. Xu, C.-C. Liu, *Adv. Funct. Mater.* **2012**, *22*, 3570; b) K. C. Poon, D. C. Tan, T. D. T. Vo, B. Khezri, H. Su, R. D. Webster, H. Sato, *J. Am. Chem. Soc.* **2014**, *136*, 5217; c) D. Kong, H. Wang, Z. Lu, Y. Cui, *J. Am. Chem. Soc.* **2014**, *136*, 4897.
[13] a) M. Liu, Y. Lu, W. Chen, *Adv. Funct. Mater.* **2013**, *23*, 1289; b) A. Zalineeva, A. Serov, M. Padilla, U. Martinez, K. Artyushkova, S. Baranton, C. Coutanceau, P. B. Atanassov, *J. Am. Chem. Soc.* **2014**, *136*, 3937; c) B. T. Sneed, C. N. Brodsky, C.-H. Kuo, L. K. Lamontagne, Y. Jiang, Y. Wang, F. Tao, W. Huang, C.-K. Tsung, *J. Am. Chem. Soc.* **2013**, *135*, 14691.
[14] a) L. Ruan, E. Zhu, Y. Chen, Z. Lin, X. Huang, X. Duan, Y. Huang, *Angew. Chem. Int. Ed.* **2013**, *52*, 12577; *Angew. Chem.* **2013**, *125*, 12809; b) S. Guo, S. Zhang, D. Su, S. Sun, *J. Am. Chem. Soc.* **2013**, *135*, 13879; c) S. M. Alia, B. S. Pivovar, Y. Yan, *J. Am. Chem. Soc.* **2013**, *135*, 13473.
[15] a) H. Li, C. Cui, S. Zhao, H. Yao, M. Gao, F. Fan, S.-H. Yu, *Adv. Energy Mater.* **2012**, *2*, 1182; b) R. Lyyamperumal, L. Zhang, G. Henkelman, R. M. Crooks, *J. Am. Chem. Soc.* **2013**, *135*, 5521; c) Y. Liang, Y. Li, H. Wang, H. Dai, *J. Am. Chem. Soc.* **2013**, *135*, 2013; d) Y. Kang, X. Ye, J. Chen, Y. Cai, R. E. Diaz, R. R. Adzic, E. A. Stach, C. B. Murray, *J. Am. Chem. Soc.* **2013**, *135*, 42.
[16] a) H.-H. Li, S. Zhao, M. Gong, C.-H. Cui, D. He, H.-W. Liang, L. Wu, S.-H. Yu, *Angew. Chem. Int. Ed.* **2013**, *52*, 7472; *Angew. Chem.* **2013**, *125*, 7620; b) Z. Peng, H. You, H. Yang, *Adv. Funct. Mater.* **2010**, *20*, 3734; c) B. Y. Xia, H. B. Wu, X. Wang, X. W. Lou, *J. Am. Chem. Soc.* **2012**, *134*, 13934; d) J. Wu, L. Qi, H. You, A. Gross, J. Li, H. Yang, *J. Am. Chem. Soc.* **2012**, *134*, 11880.
[17] a) X. Han, F. Cheng, T. Zhang, J. Yang, Y. Hu, J. Chen, *Adv. Mater.* **2014**, *26*, 2047; b) M. K. Carpenter, T. E. Moylan, R. S. Kukreja, M. H. Atwan, M. M. Tessema, *J. Am. Chem. Soc.* **2012**, *134*, 8535; c) Y. Yamauchi, A. Tonegawa, M. Komatsu, H. Wang, L. Wang, Y. Nemoto, N. Suzuki, K. Kuroda, *J. Am. Chem. Soc.* **2012**, *134*, 5100.
[18] a) C. Xu, L. Wang, R. Wang, K. Wang, Y. Zhang, F. Tian, Y. Ding, *Adv. Mater.* **2009**, *21*, 2165; b) S. Guo, S. Dong, E. Wang, *Energy Environ. Sci.* **2010**, *3*, 1307; c) H. Wang, S. Ishihara, K. Ariga, Y. Yamauchi, *J. Am. Chem. Soc.* **2012**, *134*, 10819; d) L. Wang, Y. Nemoto, Y. Yamauchi, *J. Am. Chem. Soc.* **2011**, *133*, 9674.
[19] a) B. Liu, J. Zhang, X. Wang, G. Chen, D. Chen, C. Zhou, G. Shen, *Nano Lett.* **2012**, *12*, 3005; b) X. Zhang, L. Gong, K. Liu, Y. Cao, X. Xiao, W. Sun, X. Hu, Y. Gao, J. Chen, J. Zhou, *Adv. Mater.* **2010**, *22*, 5292.
[20] a) F. Liu, S. Song, D. Xue, H. Zhang, *Adv. Mater.* **2012**, *24*, 1089; b) L. Gomez De Arco, Y. Zhang, C. Schlenker, K. Ryu, M. E. Thompson, C. Zhou, *ACS Nano* **2010**, *4*, 2865.
[21] a) Y. Xue, J. Liu, H. Chen, R. Wang, D. Li, J. Qu, L. Dai, *Angew. Chem. Int. Ed.* **2012**, *51*, 12124; *Angew. Chem.* **2012**, *124*, 12290; b) J. Luo, J. Liu, Z. Zeng, C. F. Ng, L. Ma, H. Zhang, J. Lin, Z. Shen, H. J. Fan, *Nano Lett.* **2013**, *13*, 6136.
[22] J. Feng, Q. Li, X. Lu, Y. Tong, G. Li, *J. Mater. Chem. A* **2014**, *2*, 2985.
[23] a) C. Yuan, J. Li, L. Hou, X. Zhang, L. Shen, X. W. Lou, *Adv. Funct. Mater.* **2012**, *22*, 4592; b) H. JináFan, *Energy Environ. Sci.* **2011**, *4*, 4496.
[24] Y. Lu, Y. Jiang, X. Gao, X. Wang, W. Chen, *J. Am. Chem. Soc.* **2014**, *136*, 11687.

 © 2015 Wiley-VCH Verlag GmbH & Co. KGaA, Weinheim